

Vibronic spectrum of $^{15}\text{N}^{16}\text{O}_2$ between 415 and 440 nm

E.A. Volkers^a, J. Bulthuis^a, S. Stolte^a, R. Jost^b, N. Wehres^c, H. Linnartz^{c,*}

^a Department of Physical Chemistry, Laser Centre Vrije Universiteit, De Boelelaan 1083, NL 1081 HV Amsterdam, The Netherlands

^b Laboratoire de Spectrométrie Physique, Université Joseph Fourier de Grenoble, B.P. 87, F 38402 Saint Martin d'Hères Cedex, France

^c Sackler Laboratory for Astrophysics, Leiden Observatory, Postbus 9513, NL 2300 RA Leiden, The Netherlands

Received 12 March 2007; in revised form 30 May 2007

Available online 21 July 2007

Abstract

The time gated laser induced fluorescence (LIF) excitation spectrum of adiabatically cooled $^{15}\text{N}^{16}\text{O}_2$ has been measured close to the dissociation limit (22 700–24 050 cm^{-1}). The spectrum consists of numerous rotationally resolved vibronic bands with mainly irregular structures and consequently only an angular momentum labeling has been possible. These rotationally assigned isolated transitions, however, are highly suited for laser induced dispersed fluorescence spectroscopy (LIDFS) that gives spectroscopic access to the more regular parts of the electronic $^{15}\text{N}^{16}\text{O}_2$ spectrum. Accurate lists with transition frequencies—mainly R(0) and R(2) transitions—are provided. © 2007 Elsevier Inc. All rights reserved.

Keywords: Laser spectroscopy; Supersonic jet; Nitrogen dioxide; Vibronic spectra; Isotopic effects

1. Introduction

In the last three decennia the NO_2 molecule has been topic of intense spectroscopic research. The reason for this interest is twofold. On one side NO_2 is an atmospherically relevant species known to play a key role in a number of reaction schemes, both as a buffer gas (ozone depletion), as a precursor (e.g. NO formation upon photo-dissociation) and as a reactive intermediate (e.g. in the formation of HONO or HNO_3 that are precursors of acid rain) [1]. On the other side the interpretation of the visible and near-infrared spectrum has turned out to be a spectroscopic challenge. NO_2 seems to be a rather simple molecule—three atoms and a nearly symmetric top (coat-hanger like) molecular geometry—but the electronic NO_2 spectrum is highly complex. This is due to a vibronic coupling between the X^2A_1 electronic ground state and the first electronically excited A^2B_2 state via the anti-symmetric stretch coordinate with b_2 symmetry, favored by a rather low lying conical intersection ($\sim 10\,000\text{ cm}^{-1}$) between the potential energy surfaces of these two states. In fact, NO_2 has become a prototype mol-

ecule for studies of strong intramolecular couplings and statistical approaches have been used to handle the (vibronic) level spacing distribution that have characteristics of a chaotic systems [2,3]. A number of theoretical [4–9] and experimental [10–16] studies have addressed this problem. Laser induced dispersed fluorescence spectroscopy (LIDFS) [13], laser induced fluorescence (LIF) [14], cavity ring down [15] and bolometer [16] studies have provided a wealth of spectroscopic data. For the main isotopologue $^{14}\text{N}^{16}\text{O}_2$ this has resulted recently in a simulation of the time domain non-adiabatic dynamics of the molecule on the coupled X^2A_1 and A^2B_2 electronic states [17]. So far about 300 vibronic levels below and just above the conical intersection have been vibronically assigned [13], for higher energies identifications are still ambiguous and above $16\,500\text{ cm}^{-1}$ spectra are essentially vibronically chaotic [2,3].

The majority of the electronic studies of NO_2 have focused on the main isotopic species: $^{14}\text{N}^{16}\text{O}_2$. Large gas consumption has prohibited systematic studies of the less abundant isotopologues. In an experimental article we have reported the construction of an ultra-sensitive time gated LIF setup with a gas consumption as low as $0.5\text{ }\mu\text{mol}/\text{cm}^{-1}$ spectral range [18]. This has made possible the detection of hundreds of new bands in the

* Corresponding author. Fax: +31 71 5275819.

E-mail address: linnartz@strw.leidenuniv.nl (H. Linnartz).

12000–18000 cm^{-1} region of different $^x\text{O}^y\text{N}^z\text{O}$ isotopologues, such as $^{15}\text{N}^{16}\text{O}_2$, $^{16}\text{O}^{14}\text{N}^{18}\text{O}$ and $^{14}\text{N}^{18}\text{O}_2$ [19,20]. An extension to lower energies, i.e. to the more regular part of the potential well, has not been possible, particularly because of experimental limitations, such as weak transitions and low fluorescence yields in the near infrared. The present study, however, offers a way to overcome this problem by providing LIF data of high energetic transitions of $^{15}\text{N}^{16}\text{O}_2$ as a starting point for future LIDFS work. The LIF results provide accurate excitation frequencies below the dissociation limit [21] that are needed to record high resolution dispersed fluorescence spectra similar to the work on $^{14}\text{N}^{16}\text{O}_2$ [13]. LIDFS allows access deep into the potential well and is a powerful tool even though LIDFS spectra consist of only a few rotational lines when a supersonic jet is used. The results will be complementary to direct absorption studies that probe the vibrational ground state and the lowest vibrational levels and that are available for $^{15}\text{N}^{16}\text{O}_2$ from a number of mainly Fourier transform based microwave and infrared studies [22–26].

In this letter we provide accurate excitation frequencies for the $^{15}\text{N}^{16}\text{O}_2$ isotopologue at wavelengths between 415 and 440 nm. So far more than 250 rotationally resolved vibrational bands of the $\text{A}^2\text{B}_2\text{--X}^2\text{A}_1$ electronic transition have been observed for this isotopologue in the 14300–18000 cm^{-1} region applying LIF. A full rotational analysis has been possible for the majority of these bands [19]. The present work extends $^{15}\text{N}^{16}\text{O}_2$ spectroscopy into the 22700–24050 cm^{-1} region. It should be noted that the spectroscopy at these high energies is of a different nature, as the electronic spectra are essentially rovibronically chaotic. Nevertheless, the resulting experi-

mental frequencies and the corresponding rotational assignments are a prerequisite for laser induced dispersed fluorescence experiments that are needed to access the more regular (i.e. near infrared) part of the $\text{A}^2\text{B}_2\text{--X}^2\text{A}_1$ electronic spectrum.

2. Experiment

The experimental setup has been described in detail [18]. The third harmonic of a Nd:YAG laser is used to pump a tunable dye laser covering the appropriate frequency regime using Stilbene 3 dye with a typical bandwidth of about 0.1 cm^{-1} . The laser beam is focused onto an expanding beam of a mixture of 5% $^{15}\text{N}^{16}\text{O}_2$ and Ar. The $^{15}\text{N}^{16}\text{O}_2$ is produced in a standard synthetic procedure starting from 99% pure $\text{Na}^{15}\text{NO}_3$ [19,27]. The resulting isotopic purity is better than 95%. A small gas consumption is achieved by using a high intensity piezo electric pulsed molecular beam source that is optimized for a well-defined short pulse shape with an opening time of 150 μs . A photomultiplier tube, sensitive for 310–860 nm, is used to monitor the fluorescence zone that is about 1.5 cm downstream from the nozzle orifice. Cut-off filters are used to shield the detector from residual laser light. Typically 10 laser shots are averaged for each data point. The bandwidth of the pulsed laser system is the limiting factor in determining the absolute frequency accuracy for which a wavemeter is used. A conservative estimate yields an absolute frequency accuracy of 0.05 cm^{-1} . As the setup has been designed for fully automatic scanning over large frequency ranges an etalon signal with a free spectral range of 1.22 cm^{-1} is recorded to correct for non-linearities.

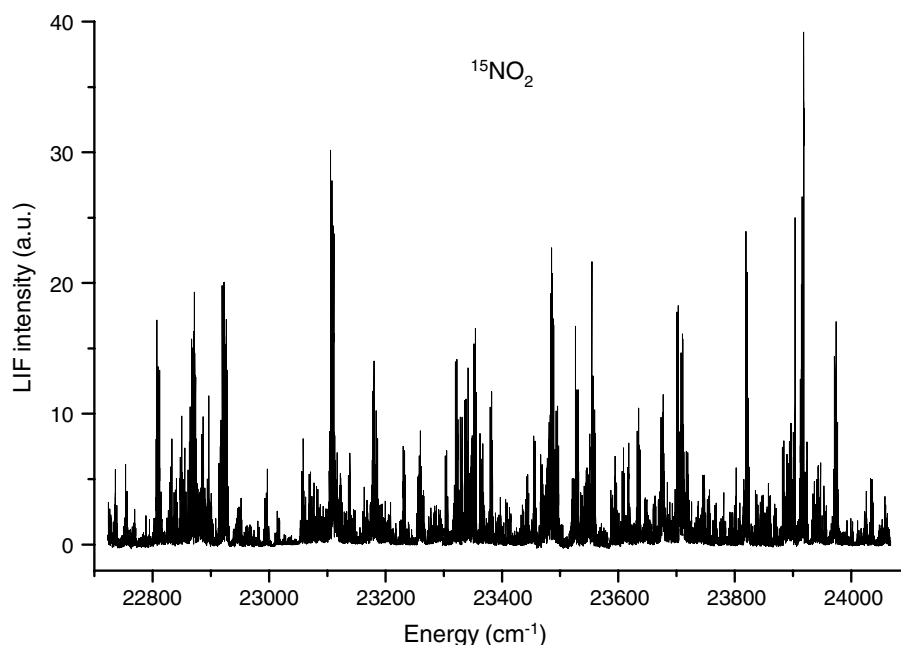


Fig. 1. An overview scan of the electronic spectrum of $^{15}\text{N}^{16}\text{O}_2$ in the 415–440 nm region recorded by time gated LIF spectroscopy. The intensities are normalized on the absorption cross section (assuming constant fluorescence detection efficiency). The general features (spectral density and intensity distribution) are similar to those previously observed for the main isotopologue.

3. Results and discussion

In Fig. 1 an overview spectrum is shown of the 415–440 nm region using LIF spectroscopy.

In total, about one hundred vibronic bands due to the $A^2B_2-X^2A_1$ electronic transition of $^{15}N^{16}O_2$ are found. The bands vary in intensity and in spectral appearance. The overall intensity profile of the raw data follows the dye efficiency curve. Therefore, the relative intensities in Fig. 1 have been normalized to reproduce, after smoothing, the absorption cross section, in a similar way as for the main isotopologue [28–30] where it was shown that the ratio between smoothed LIF intensities and absorption cross sections yields a constant ratio. The majority of the observed $^{15}N^{16}O_2$ bands are rotationally resolved. A zoomed spectrum is shown in Fig. 2 and clearly shows a rotational structure. The rotational labeling is indicated and is based upon combination differences, linking the line positions to well-known ground state values [24–26]. The small number of transitions is due to rotational cooling in the jet expansion, yielding a rotational temperature T_{rot} typically between 5 and 10 K [18–20]. Particularly the R(0) and R(2) transitions are of relevance for LIDFS measurements as these are linked via selection rules to the $J = 1/2$, $3/2$, and $5/2$ levels in the electronic ground state. It should be noted that for symmetric $^xO^yN^xO$ isotopes (i.e. $^{15}N^{16}O_2$) only even N -levels ($N = J + 1/2$ or $J - 1/2$) are symmetry allowed for $K = 0$ bands. Obviously, for each R(0) line a corresponding P(2) line exists that is red shifted by 2.52 cm^{-1} ($\sim 6B$) and with an intensity equal within 30% of that found for the R(0) transition. Similarly, for each R(2) transition a P(4) line can be assigned, red shifted by 5.88 cm^{-1} ($\sim 14B$) and with a much weaker intensity. These P-transitions are not listed in Table 1.

Besides the rotational structure, some bands also show electronic spin splitting and, for strong vibronic transitions, not only $K = 0$ but also $K = 1$ transitions are observed. In Refs. [19,20] it has been shown how such bands are treated spectroscopically and what difficulties one may expect. However, the goal of the present work is not a systematic fit of individual bands, particularly as spectral irregularities are more a rule than an exception in this high energy range, but to provide accurate ($<0.05 \text{ cm}^{-1}$) line positions as well as rotational assignments in order to present the strongest transitions suited for LIDFS measurements. The results are summarized in Table 1.

The S/N ratio of the three stronger rotational transitions in Fig. 2 (P(2), R(0) and R(2)) is about 50. This band (#2 Table 1) is located near the edge of the Stilbene 3 dye curve. For this reason, the S/N ratio of this band is lower than most of the other observed vibronic bands. However, this band has a rather strong intrinsic intensity as indicated in the last column of Table 1. Most of the recorded bands are not as regular as the one shown in Fig. 2. Because of rovibronic interactions [31] with resulting spin splitting and extra-lines, it is possible that perturbed vibronic bands of significant intensity have not been recognized and are missing in Table 1. In addition, rovibronic perturbations are also reflected in the table where sometimes only the R(0) transition or only the R(2) transition is listed for a specific band. This means that the upper levels of the missing transitions are perturbed, resulting in weaker transitions that are below our arbitrary threshold of 5% of the strongest transition. In some cases the two spin components are resolved and the resulting line positions are then given in the table.

The 68 listed bands which do not involve any hot bands—these can be neglected in this high energy range

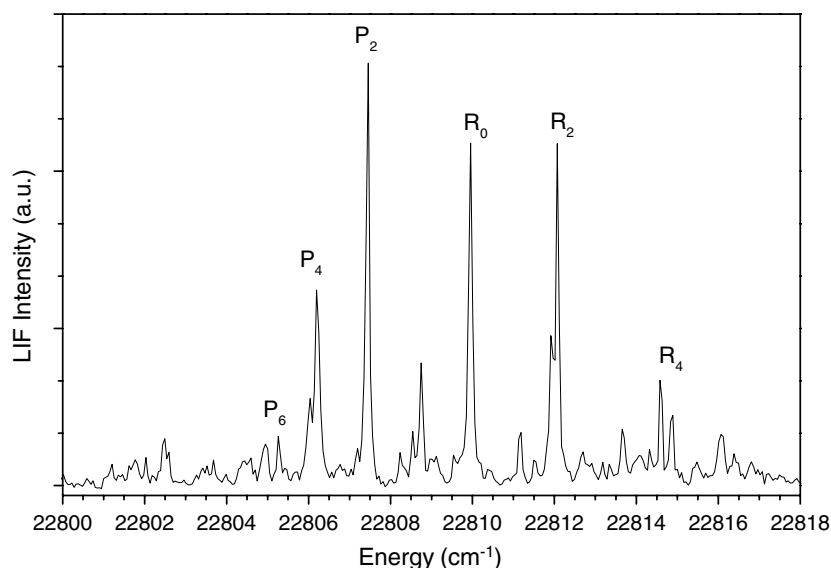


Fig. 2. A zoomed spectrum of band #2 (Table 1) around 22809 cm^{-1} . The spectrum consists of low rotational transitions, R(0)–P(2), R(2)–P(4) of the $K = 0$ sub-band and some weak and unidentified lines that most likely relate to transitions starting from higher K ($K > 0$) and N ($N > 4$) values. The assignment for the stronger transitions follows the use of combination differences. The band is one of the few more regular bands in this blue region. The S/N ratio is limited by low laser power as the absorption frequency is close to the end of the dye enhancement curve.

Table 1

List of identified R(0) and R(2) transitions of $^{15}\text{N}^{16}\text{O}_2$ in the 415–440 nm region for 68 different bands with observed S/N ratios better than typically 50

Nos.	ω_c [cm^{-1}]	Transition	Intensity [a.u.]
1	22756.02	R(0)	16
2	22809.95	R(0)	54
	22812.08	R(2)	53
3	22831.30	R(0)	24
	22833.22	R(2)	32
4	22839.42	R(0)	16
	22840.87	R(2)	15
	22841.26	R(2)	20
5	22849.96	R(0)	25
6	22855.21	R(0)	22
7	22863.21	R(0)	23
	22864.51	R(2)	27
8	22871.24	R(0)	40
	22872.66	R(2)	48
9	22922.18	R(0)	50
	22923.14	R(2)	50
	22923.40	R(2)	40
10	22925.25	R(0)	27
	22926.62	R(2)	42
	22927.38	R(2)	25
11	22995.58	R(0)	10
	22996.96	R(2)	14
12	23058.69	R(0)	14
	23058.88	R(0)	20
13	23107.95	R(0)	40
	23108.26	R(0)	70
	23110.02	R(2)	61
	23110.40	R(2)	52
14	23139.04	R(0)	17
15	23147.86	R(0)	8
16	23163.55	R(0)	11
17	23180.05	R(0)	35
	23181.14	R(0)	26
18	23186.23	R(2)	20
19	23232.93	R(0)	18
	23233.56	R(2)	13
20	23258.11	R(0)	17
	23259.65	R(2)	22
	23261.49	R(0)	15
21	23305.18	R(0)	18
	23306.57	R(2)	8
	23306.79	R(2)	10

Table 1 (continued)

Nos.	ω_c [cm^{-1}]	Transition	Intensity [a.u.]
22	23322.74	R(0)	35
	23324.30	R(2)	24
23	23331.36	R(0)	25
	23332.52	R(2)	12
24	23338.42	R(0)	28
	23339.54	R(0)	10
	23339.87	R(0)	19
25	23354.14	R(0)	22
	23354.47	R(0)	41
	23355.95	R(2)	29
	23356.12	R(2)	20
26	23364.92	R(0)	16
	23367.32	R(2)	19
27	23382.25	R(0)	29
	23382.53	R(0)	8
	23383.65	R(2)	20
28	23397.30	R(0)	9
	23398.19	R(2)	5
29	23408.97	R(0)	8
	23410.36	R(2)	5
30	23415.27	R(0)	5
31	23435.37	R(0)	8
	23436.59	R(2)	7
32	23443.00	R(0)	12
	23444.49	R(2)	13
33	23456.86	R(0)	20
	23458.54	R(2)	7
34	23468.81	R(0)	10
	23469.11	R(0)	18
	23470.00	R(2)	10
	23470.26	R(2)	13
35	23486.66	R(0)	52
	23487.69	R(0)	42
	23489.02	R(2)	41
36	23495.74	R(0)	26
	23497.29	R(2)	18
	23497.47	R(2)	10
37	23528.93	R(0)	30
	23530.96	R(2)	30
38	23559.10	R(0)	26
39	23590.28	R(0)	9
	23590.56	R(0)	5
	23593.20	R(2)	8
40	23596.77	R(0)	12
	23596.94	R(0)	13
	23598.47	R(2)	7

Table 1 (continued)

Nos.	ω_c [cm ⁻¹]	Transition	Intensity [a.u.]
41	23609.03	R(0)	18
	23610.17	R(2)	14
42	23634.98	R(0)	26
	23635.44	R(0)	19
	23636.35	R(2)	10
	23636.94	R(2)	18
43	23662.46	R(0)	8
	23662.76	R(0)	10
	23662.95	R(0)	7
	23663.12	R(2)	10
	23663.64	R(2)	5
	23664.41	R(2)	7
44	23675.81	R(0)	25
	23676.15	R(0)	23
	23677.94	R(0)	17
45	23703.08	R(0)	45
	23705.03	R(2)	21
46	23710.27	R(0)	40
	23710.82	R(0)	39
	23712.04	R(2)	23
	23712.54	R(2)	17
47	23719.01	R(0)	17
	23719.70	R(2)	6
	23720.04	R(2)	13
48	23735.95	R(0)	8
49	23747.45	R(0)	13
	23747.89	R(0)	11
	23748.16	R(0)	10
	23749.56	R(2)	7
50	23755.17	R(0)	9
	23756.76	R(0)	11
51	23764.95	R(0)	5
	23766.46	R(2)	5
52	23767.88	R(0)	8
53	23779.16	R(0)	5
	23780.88	R(2)	10
54	23802.10	R(0)	10
	23802.47	R(2)	18
55	23821.72	R(0)	52
	23822.52	R(0)	28
	23823.04	R(0)	10
	23823.34	R(2)	20
56	23838.08	R(0)	10
57	23846.55	R(0)	9
	23847.33	R(2)	7
	23848.54	R(2)	10
58	23853.33	R(0)	7
	23854.22	R(0)	5

Table 1 (continued)

Nos.	ω_c [cm ⁻¹]	Transition	Intensity [a.u.]
59	23860.18	R(0)	9
	23861.58	R(2)	10
60	23884.26	R(0)	20
61	23917.20	R(0)	56
	23917.95	R(0)	85
	23918.28	R(2)	100
62	23936.67	R(0)	12
63	23943.56	R(0)	18
64	23955.75	R(0)	9
	23957.16	R(2)	8
65	23973.88	R(0)	42
	23976.16	R(2)	23
66	24002.10	R(0)	5
	24003.31	R(2)	3
67	24025.66	R(0)	10
	24026.69	R(2)	5
68	24035.47	R(0)	12
	24036.03	R(0)	8
	24037.00	R(2)	9
	24037.39	R(2)	8

The band number (#) is indicated in the first column. The absolute line positions (second column) are accurate up to 0.05 cm⁻¹. The relative line intensities (last column) are given in % of the R(2) line intensity at 23918.28 cm⁻¹ (#61).

(see Ref. [3])—represent about 20% of the total number of 350 ²B₂ vibronic transitions expected in this range [2,3]. They convey about 80% of the total intensity as can be concluded from the table in which line intensities are given in % of the strongest observed line, the R(2) transition of a band located at 23918.28 cm⁻¹ (# 61 Table 1). The distribution of these intensities is close to a Porter-Thomas distribution [32] and also this compares well with previous observations for the main isotopologue ¹⁴N¹⁶O₂.

Currently, there is much interest in understanding the electronic spectrum of NO₂. In the case of the main ¹⁴N¹⁶O₂ isotopologue LIDFS measurements have provided information on energy levels deep in the potential well and from these it has been possible to extend new models to increasingly higher energies [33]. The data set presented here makes it possible to start similar LIDFS work on the ¹⁵N¹⁶O₂ isotopologue. A direct comparison between the two systems provides additional information; the vibrational and rotational spacings will differ, reflecting the minor differences in molecular masses, and intensities of similar bands may vary substantially because of large changes in the eigenstate mixing coefficients due to changes in the vibronic energies. An extension to LIDFS studies of other isotopologues is challenging, particularly the

asymmetric isotopologues $^{18}\text{O}^{14}\text{N}^{16}\text{O}$ and $^{18}\text{O}^{15}\text{N}^{16}\text{O}$ as the two sets (A_1 and B_2) of vibronic levels merge into a single set of A' symmetry (C_s group).

In summary; this work presents for the first time a systematic study of rotationally resolved vibronic bands of $^{15}\text{N}^{16}\text{O}_2$ in a high energy range ($22\,700\text{--}24\,050\text{ cm}^{-1}$) close to the dissociation limit. Even though the bands cannot be spectroscopically fitted, a large number of accurate $R(0)$ and $R(2)$ line positions has become available that are a prerequisite to start LIDFS measurements to access lower lying and more regular vibronic transitions of $^{15}\text{N}^{16}\text{O}_2$.

Acknowledgments

Financial support by the Netherlands Organization for Scientific Research (NWO) is acknowledged through FOM and NOVA. R.J., who belongs to ENSPG-INP Grenoble, acknowledges EU support within the integrating infrastructure initiative: contract RII3-CT-2003-506350.

References

- [1] R.C. Cohen, J.G. Murphy, *Chem. Rev.* 103 (2003) 4985–4998.
- [2] A. Delon, R. Jost, M. Lombardi, *J. Chem. Phys.* 95 (1991) 5701–5718.
- [3] R. Georges, A. Delon, R. Jost, *J. Chem. Phys.* 103 (1995) 1732–1747.
- [4] E. Haller, H. Koppel, L.S. Cederbaum, *J. Mol. Spectrosc.* 111 (1985) 377–397.
- [5] D.M. Leitner, H. Koppel, L.S. Cederbaum, *J. Chem. Phys.* 104 (1996) 434–443.
- [6] E. Leonardi, C. Petrongolo, G. Hiersch, R.J. Buenker, *J. Chem. Phys.* 105 (1996) 9051–9067.
- [7] R.F. Salzgeber, V.A. Mandelshtam, C. Schlier, H.S. Taylor, *J. Chem. Phys.* 110 (1999) 3756–3764.
- [8] S. Mahapatra, H. Koppel, L.S. Cederbaum, P. Stampfuss, W. Wenzel, *Chem. Phys.* 259 (2000) 211–226.
- [9] A.J.C. Varandas, *J. Chem. Phys.* 119 (2003) 2596–2613.
- [10] R.E. Smalley, L. Wharton, D.H. Levy, *J. Chem. Phys.* 63 (1975) 4977–4989.
- [11] G. Persch, H.J. Vedder, W. Demtröder, *Chem. Phys.* 105 (1986) 471–479.
- [12] F. Bylicki, G. Persch, E. Mehdizadeh, W. Demtröder, *Chem. Phys.* 135 (1989) 255–265.
- [13] B. Kirmse, A. Delon, R. Jost, *J. Chem. Phys.* 108 (1998) 6638–6651.
- [14] A. Delon, R. Jost, *J. Chem. Phys.* 110 (1999) 4300–4308.
- [15] D. Romanini, P. Dupre, R. Jost, *Vib. Spectrosc.* 19 (1999) 93–106.
- [16] C.A. Biesheuvel, D.H.A. ter Steege, J. Bulthuis, M.H.M. Janssen, J.G. Snijders, S. Stolte, *Chem. Phys. Lett.* 269 (1997) 515–522.
- [17] M. Sanrey, M. Joyeux, *J. Chem. Phys.* 126 (2007) 074301 (1–9).
- [18] E.A. Volkers, A. Vredenburg, H. Linnartz, J. Bulthuis, S. Stolte, R. Jost, *Chem. Phys. Lett.* 391 (2004) 106–111.
- [19] E.A. Volkers, M.C. Koudijzer, A. Vredenburg, J. Bulthuis, S. Stolte, H. Linnartz, R. Jost, *J. Mol. Spectrosc.* 235 (2006) 1–17.
- [20] E.A. Volkers, J. Bulthuis, S. Stolte, R. Jost, H. Linnartz, *J. Mol. Spectrosc.* 238 (2006) 11–22.
- [21] G. Michalski, R. Jost, D. Sugny, M. Joyeux, M. Thiemens, *J. Chem. Phys.* 121 (2004) 7153–7161.
- [22] J.C.D. Brand, P.H. Chiu, A.R. Hoy, *Can. J. Phys.* 57 (1979) 828–835.
- [23] Y. Morino, M. Tanimoto, S. Saito, E. Hirota, R. Awata, T. Tanaka, *J. Mol. Spectrosc.* 98 (1983) 331–348.
- [24] Y. Hamada, *J. Mol. Struct.* 242 (1991) 367–377.
- [25] J. Orphal, A. Perrin, J.-M. Flaud, M. Smirnov, S. Himmelmann, S. Voigt, J.P. Burrows, *J. Mol. Spectrosc.* 204 (2000) 72–79.
- [26] S. Miljanic, A. Perrin, J. Orphal, *J. Mol. Spectrosc.* 243 (2007) 176–181 (and references therein).
- [27] A. Pedler, F.H. Pollard, in: T. Moeller (Ed.), *Inorganic Syntheses*, vol. V, McGraw-Hill, New York, 1957, p. 87.
- [28] Unpublished results from the Grenoble group.
- [29] L.S. Rothman, D. Jacquemart, A. Barbe, D. Chris Benner, M. Birk, L.R. Brown, M.R. Carleer, C. Chackerian Jr., K. Chance, L.R. Coudert, V. Dana, V.M. Devi, J.-M. Flaud, R.R. Gamache, A. Goldman, J.-M. Hartmann, K.W. Jucks, A.G. Maki, J.-Y. Mandin, S.T. Massie, J. Orphal, A. Perrin, C.P. Rinsland, M.A.H. Smith, J. Tennyson, R.N. Tolchenov, R.A. Toth, J. Vander Auwera, P. Varanasi, G. Wagner, *J. Quant. Spectrosc. Radiat. Transfer* 96 (2005) 139–204.
- [30] A.C. Vandaele, C. Hermans, P.C. Simon, M. Carleer, R. Colin, S. Fally, M.F. Merienne, A. Jenouvrier, B. Coquart, *J. Quant. Spectrosc. Radiat. Transfer* 59 (1998) 171–184.
- [31] A. Delon, R. Georges, R. Jost, *J. Chem. Phys.* 103 (1995) 7740–7773.
- [32] T.A. Brody, J. Flores, J.B. French, P.A. Mello, A. Pandey, S.S.M. Wong, *Rev. Mod. Phys.* 53 (1981) 385–479.
- [33] M. Joyeux, R. Jost, M. Lombardi, *J. Chem. Phys.* 119 (2003) 5923–5932.